Emergence of functional subnetworks in layer 2/3 cortex induced by sequential spikes in vivo

Taekeun Kim[a,1,2], Won Chan Oh[a,1], Joon Ho Choi[a], and Hyung-Bae Kwon[a,b,3]

[a]Max Planck Florida Institute for Neuroscience, Jupiter, FL 33458; and [b]Max Planck Institute of Neurobiology, 82152 Martinsried, Germany

Edited by Gina G. Turrigiano, Brandeis University, Waltham, MA, and approved January 29, 2016 (received for review July 8, 2015)

During cortical circuit development in the mammalian brain, groups of excitatory neurons that receive similar sensory information form microcircuits. However, cellular mechanisms underlying cortical microcircuit development remain poorly understood. Here we implemented combined two-photon imaging and photolysis in vivo to monitor and manipulate neuronal activities to study the processes underlying activity-dependent circuit changes. We found that repeated triggering of spike trains in a randomly chosen group of layer 2/3 pyramidal neurons in the somatosensory cortex triggered long-term plasticity of circuits (LTPc), resulting in the increased probability that the selected neurons would fire when action potentials of individual neurons in the group were evoked. Significant firing pattern changes were observed more frequently in the selected group of neurons than in neighboring control neurons, and the induction was dependent on the time interval between spikes, N-methyl-D-aspartate (NMDA) receptor activation, and Calcium/calmodulin-dependent protein kinase II (CaMKII) activation. In addition, LTPc was associated with an increase of activity from a portion of neighboring neurons with different probabilities. Thus, our results demonstrate that the formation of functional microcircuits requires broad network changes and that its directionality is nonrandom, which may be a general feature of cortical circuit assembly in the mammalian cortex.

spike timing-dependent plasticity | layer 2/3 cortex | neuronal connectivity

Layer 2/3 neurons in the barrel cortex play a central role in integrative cortical processing (1–4). Neurons in layer 2/3 are interconnected with each other, and their axons and dendrites traverse adjacent barrel areas (5, 6). Recent calcium (Ca^{2+}) imaging studies in awake animals showed that two very closely localized layer 2/3 pyramidal neurons are independently activated by different whiskers (7). In addition, adjacent layer 2/3 neurons have different receptive field properties; signals from different whiskers may emerge on different spines in the same neurons (8, 9). These findings suggest that the organization of functional subnetworks in somatosensory layer 2/3 is heterogeneous at the single-cell level and that microcircuits are assembled at a very fine scale (10). In vivo whole-cell recording experiments have also shown that most, but not all, layer 2/3 pyramidal neurons receive subthreshold depolarization by single-whisker stimulation with much broader receptive fields than neurons in layer 4 (11, 12). These anatomical and functional data suggest that electric signals relayed to the cortex by whisker activation are greatly intermingled within layer 2/3 neurons, and that studying the mechanisms by which these layer 2/3 neurons make connections may be critical for understanding the cortical network organizing principles underlying somatosensation.

A previous modeling study suggested that spike timing-dependent plasticity (STDP) can lead to the formation of functional cortical columns and activity-dependent reorganization of neural circuits (13–16). However, how spikes arising in multiple neurons in vivo influence their connectivity is poorly understood. In this study using two-photon glutamate photolysis, which allowed us to control neuronal activity in a spatially and temporally precise manner, we examined activity-dependent cellular mechanisms during network rearrangement generated by repetitive spike trains in a group of neurons. We found that repetitive spikes on a group of neurons induced the probability of the neurons firing together. This circuit plasticity required spiking at short intervals among neurons and is expressed by N-methyl-D-aspartate (NMDA) receptor- and Calcium/calmodulin-dependent protein kinase II (CaMKII)-dependent long-lasting connectivity changes. The probability of firing was differentially affected by the order of the spike sequence but was not dependent on the physical distance between neurons. Thus, our data show that neuronal connectivity within a functional subnetwork is established in not only a preferred but also a directional manner.

Results

Two-Photon Glutamate Photolysis Triggers Action Potentials in Vivo. We first verified whether we could use photolysis of caged glutamate to control neuronal activity at single-cell resolution. We injected adeno-associated virus expressing GCaMP6f (AAV1 Syn GCaMP6f) into mouse layer 2/3 somatosensory cortex (postnatal days 11–13) (Fig. 1*A*) (17). Ten to 21 d after viral injection, we observed many neurons expressing green fluorescence using two-photon laser-scanning microscopy at 910-nm wavelength (Fig. 1 *B* and *C*). To test whether we could detect Ca^{2+} transients by triggering action potentials (APs) from single neurons, we circulated 2.5 mM 4-carboxymethoxy-5,7-dinitroindolinyl-glutamate (CDNI-Glu) within the microchamber (*SI Appendix*, Fig. S1 *A* and *B*) and then photolyzed CDNI-Glu at the edge of the cell body for 2 ms at a wavelength of 720 nm (Fig. 1*D*) (18). Significant amounts of Ca^{2+} transients were observed from the target neuron upon uncaging (Fig. 1*D*). The spatial precision of Ca^{2+} responses triggered by two-photon glutamate photolysis was very high, such that redirecting

Significance

Somatosensory information is transmitted and processed in the superficial layer (layer 2/3) of the cortex, giving rise to proper sensory perception. These processes ought to be dependent on the patterns of neuronal connectivity among layer 2/3 neurons, but underlying cellular mechanisms that govern how one neuron makes specific connections with other neurons and eventually builds functional microcircuits are not fully understood. We found that spikes generated in multiple neurons in vivo induced the formation of a functional group of neurons. Further data demonstrated that functional connectivity was determined by the order of the spike sequence and the number of neurons but not by the physical distance among neurons. These results imply that time-sensitive neuronal activity determines the pattern of circuit connectivity.

Author contributions: T.K., W.C.O., and H.-B.K. designed research; T.K., W.C.O., and J.H.C. performed research; T.K. and W.C.O. analyzed data; and H.-B.K. wrote the paper.

The authors declare no conflict of interest.

This article is a PNAS Direct Submission.

[1]T.K. and W.C.O. contributed equally to this work.

[2]Present address: Department of Brain and Cognitive Sciences, Massachusetts Institute of Technology, Cambridge, MA 02139.

[3]To whom correspondence should be addressed. Email: hyungbae.kwon@mpfi.org.

This article contains supporting information online at www.pnas.org/lookup/suppl/doi:10.1073/pnas.1513410113/-/DCSupplemental.

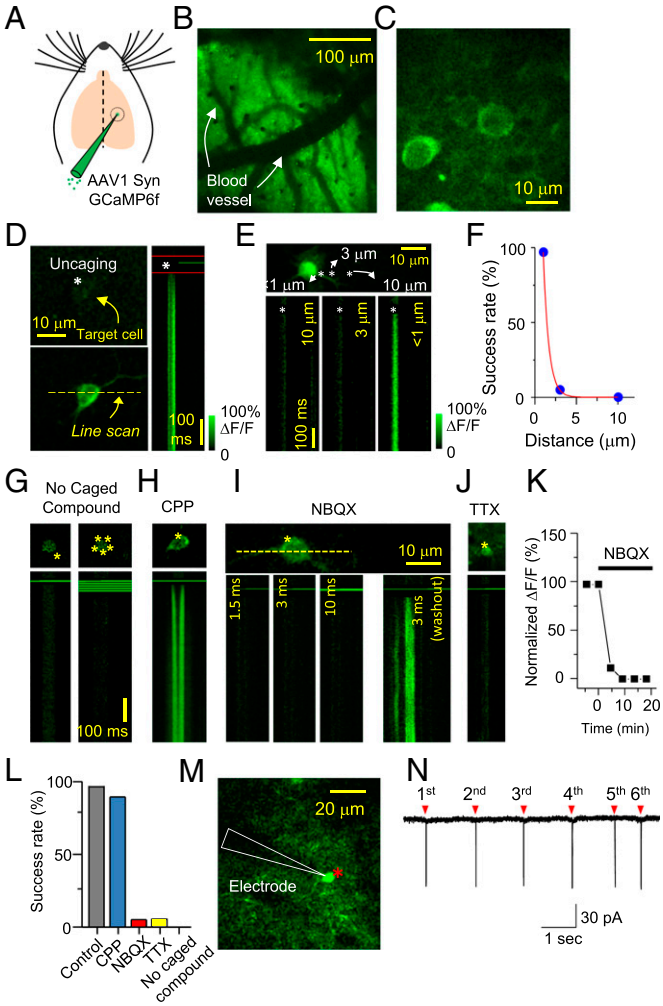

Fig. 1. Simultaneous in vivo two-photon imaging and photolysis. (*A*) AAV expressing GCaMP6f (0.3 μL) was injected into layer 2/3 primary somatosensory cortex. (*B*) Low-magnification image through a cranial window (300 × 300 μm) 2~3 wk after viral injection. (*C*) Individual GCaMP6 virus-infected neurons were visible under high magnification. (*D*) Glutamate photolysis onto a single cell. A yellow dotted line indicates where the line scan was performed, and asterisks indicate the uncaging spot. The imaging laser light path was blocked in the time period between the two red lines. (*E*) Glutamate uncaging 10, 3, and 1 μm away from the cell body while doing a line scan. (*F*) Plot of the distance-dependent success rate of Ca^{2+} transients. (*G*) Two-photon excitation without caged compounds. Single- or multiple-spot uncaging light surrounding the cell body did not trigger any noticeable Ca^{2+} transients even with a longer duration of light (10 ms) ($n = 15$). (*H*) Robust Ca^{2+} rise was triggered in the presence of the selective NMDA receptor antagonist CPP (200 μM). (*I*) Blockade of AMPA receptor with NBQX (1 mM) nearly completely blocked Ca^{2+} transients, but photolysis of glutamate 30 min after NBQX washout successfully evoked Ca^{2+} rise from the same cell, indicating that Ca^{2+} rise was dependent on the activation of AMPA receptors. (*J*) TTX (100 μM) prevented Ca^{2+} transients. (*K*) Time course graph of Ca^{2+} signal blockade by NBQX application. (*L*) Summary graph of the success rate in Ca^{2+} transients evoked by two-photon uncaging ($n = 45$ for CPP; $n = 16$ for NBQX; $n = 31$ for TTX; $n = 9$ for no caged compound). (*M*) Representative picture of an in vivo cell-attached recording when the target neuron was activated by glutamate uncaging (asterisk). (*N*) Six successive glutamate photolyses (red triangles) triggered action potentials from the target neuron repetitively.

the 720-nm light 3 μm away from the cell body failed to elicit any Ca^{2+} transients (Fig. 1*E*). This micron-level resolution in the *x*–*y* plane is consistent with previous studies using in vitro brain slices (19–21). We were able to achieve high reliability with this light-induced control of Ca^{2+} activity, with a success rate of ~97% (Fig. 1*F*). To test whether the activity of each neuron could be controlled precisely even in areas where a large number of neurons were intermingled, we picked two neurons several microns apart and photolyzed glutamate onto each cell separately. Ca^{2+} transients were triggered only in the target cell without inducing Ca^{2+} rises in the other cell (*SI Appendix*, Fig. S1 *C* and *D*).

These data strongly indicate that simultaneous in vivo uncaging and imaging has the precision required to stimulate and record the activity of individual neurons in vivo. Genetically encoded calcium indicators have been used to detect Ca^{2+} influx elicited by APs (17, 22, 23). Therefore, the observed Ca^{2+} transients likely represent neuronal spiking. To determine whether glutamate uncaging onto neurons triggers APs, we further characterized the system using pharmacology. First, we confirmed that Ca^{2+} transients originated from the activation of glutamate receptors. In the absence of CDNI-Glu, no Ca^{2+} transients were detected (Fig. 1*G*). To distinguish which glutamate receptors mediate APs and Ca^{2+} signals, we blocked NMDA or α-amino-3-hydroxy-5-methyl-4-isoxazolepropionic acid (AMPA) receptors with the selective antagonists (RS)-3-(2-carboxypiperazin-4-yl)-propyl-1-phosphonic acid (CPP) or 2,3-Dioxo-6-nitro-1,2,3,4-tetrahydrobenzo[f]quinoxaline-7-sulfonamide (NBQX), respectively, and found that AMPA receptor activation was necessary for cell firing and Ca^{2+} activity (Fig. 1 *H*, *I*, *K*, and *L*). Blockade of sodium channels with Tetrodotoxin (TTX) also prevented any rises in Ca^{2+} (Fig. 1 *J* and *L*). These pharmacological experiments indicate that glutamate photolysis triggers APs via AMPA receptor activation. We also gradually increased the laser power and observed all-or-none Ca^{2+} transients similar to AP firing, further supporting that the Ca^{2+} responses in our experiments arose mainly from neuronal APs rather than subthreshold depolarization in the cell body (*SI Appendix*, Fig. S1*E*). Last, we recorded APs in response to glutamate uncaging by in vivo cell-attached recording (*SI Appendix*, Fig. S1*F*). The success rate and spatial precision of APs were similar to those observed using Ca^{2+} imaging (*SI Appendix*, Fig. S1*G*), and we could trigger repetitive APs reliably (Fig. 1 *M* and *N*).

We next tested whether glutamate uncaging could activate (*i*) multiple neurons located right above or below the target neurons or (*ii*) layer 5 neurons by activating their dendrites. To do so, we patched one neuron and released glutamate 10–20 μm above or below the target neuron. We found that glutamate release 10 μm above or below the cell soma did not cause APs in neurons (Fig. 2 *A* and *B*). Because the soma size is about 10 μm, the chance of activating other neurons located right above or below the target cell is very low; however, if another cell is located within 10 μm, it is possible that more than one neuron can fire via glutamate uncaging. When we released glutamate at several locations of distal apical dendrites of layer 5 neurons, APs were triggered with a success rate of less than 10% (Fig. 2 *C* and *D*). Therefore, there is only a small possibility that layer 5 neurons will be activated in our study.

Repetitive Triggering of Spike Trains in a Group of Neurons Induced Functional Circuit Rearrangement. Neurons tend to wire together when similar sensory inputs activate a subset of neurons repetitively, but how this occurs and eventually yields ensembles of neurons with similar functions is unclear. It is improbable that this process is random; thus, there are likely a trigger or igniting point to initiate this process and specific rules to connect discrete subpopulations of neurons. STDP has been regarded as a central cellular mechanism of circuit plasticity in various brain areas including the somatosensory cortex (24, 25), visual cortex (26), and hippocampus (27). In an initial set of experiments, we developed a sequential activation paradigm for inducing plasticity in intact cortical circuits similar to STDP. Using glutamate photolysis, we sequentially triggered APs in seven closely localized neurons at 10-ms intervals (Fig. 3*A*). This sequential activation was repeated three times followed by a 2-min rest. These 3 sequential activa-

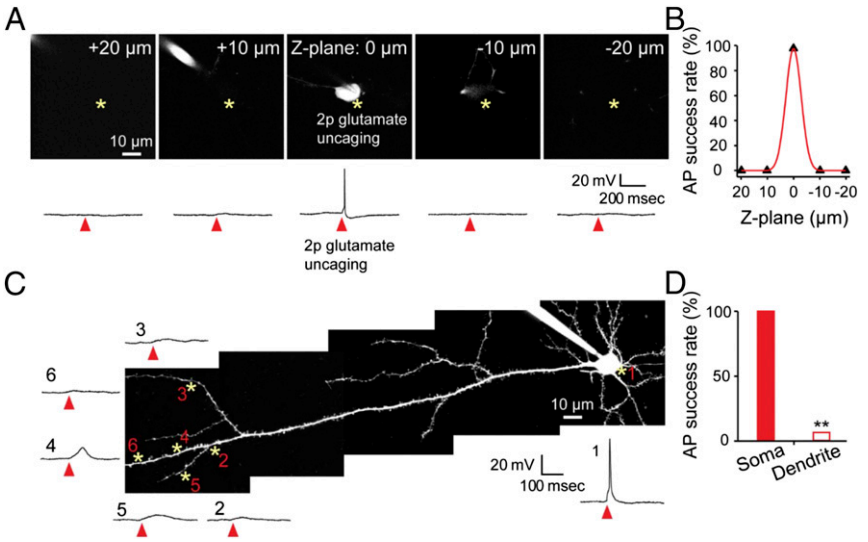

Fig. 2. *Z* resolution of glutamate uncaging-induced action potentials and comparison between soma and dendritic uncaging. (*A*) Representative images of focal planes at 20, 10, 0, −10, and −20 μm from the target neuron (*Top*) and current-clamp recording traces (*Bottom*). A cortical layer 2/3 pyramidal neuron from slice culture was loaded with 200 μM Alexa 488 through the recording electrode to visualize the cell. Asterisks indicate glutamate uncaging. (*B*) Summary plot of the AP success rate at different *Z*-focal planes ($n = 4$ neurons). (*C*) Representative image of a layer 5 pyramidal neuron and sample traces evoked by glutamate uncaging are plotted. Note that glutamate uncaging at the cell body triggered action potentials but not by uncaging at the dendrite. Asterisks indicate glutamate uncaging sites, and arrowheads indicate glutamate uncaging time points. (*D*) Summary graph of the AP success rate between the soma and dendrite ($n = 3$ neurons, 32 uncaging trials at the dendrite). $^{**}P < 0.01$; error bars are SEM.

tions/2-min rest intervals were repeated 15 times for a total of 45 (3 × 15) sequential activations. Before initiating this induction procedure, we detected Ca^{2+} transients only from the neuron that received glutamate photolysis (Fig. 3*B*), suggesting that APs in one neuron are not strong enough to trigger firing in neighboring neurons or that they are not synaptically connected. Interestingly, repetitive firing in several neurons in sequence caused a significant increase in the level of Ca^{2+} transients from other neurons in the selected group (Fig. 3 *B–D* and *SI Appendix*, Table S1; $P < 0.05$). Thus, glutamate uncaging on the target neuron triggered a Ca^{2+}

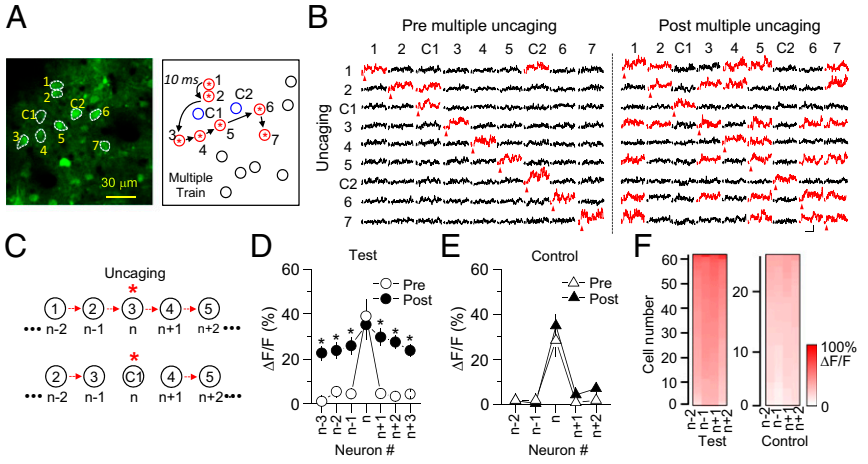

Fig. 3. Formation of a group of neurons firing together induced by repetitive triggering of spike trains. (*A*) Representative image of a group of neurons labeled in an arbitrary way. C1 and C2 indicate control neurons located near the subgroup of neurons, but APs at those neurons were not triggered by photolysis. Glutamate photolysis was given in sequence as labeled by numbers at a 10-ms interval. This sequential activation was repeated three times successively. Then these 3× spike trains were repeated 15 times at 2-min intervals, making a total of 45 spike trains. Blue circles, neighboring control neurons included in the imaging; black circles, neighboring control neurons not included in the imaging; red/asterisk circles, target neurons. (*B*) Time courses of Ca^{2+} transients from all neurons within the activated group and control neurons are plotted before and after multiple spike trains. When Ca^{2+} transients were triggered from the target neurons, fluorescence changes were monitored in all other neurons, including control neurons, simultaneously. Neurons showing more than 20% change of $\Delta F/F$ are marked as red traces. (Scale bars, 50% and 200 ms.) (*C*) Schematic diagram of numbering for data analysis. The target neuron was always called "n." The neuron that was activated 10 ms before the target neuron was labeled n−1, and n−2 was the neuron we activated 20 ms before the target neuron. n+1, n+2,... were labeled in a similar way but to the opposite direction. The closest neuron from the control neuron was also labeled in a similar way as shown in *A*. Red arrows indicate glutamate uncaging. Asterisks indicate glutamate uncaging. (*D*) Comparison of fluorescence changes between pre and post repetitive spike trains. (*E*) Summary graph of fluorescence changes when control neurons were activated. * indicates statistical significance ($P < 0.05$) and error bars represent SEM. (*F*) Color code analysis showing that $\Delta F/F$ is slightly higher in neurons closer to the target neuron in the test condition but not in the control condition.

rise not only in the target neuron but also in other neurons within the group, suggesting the formation of functional microcircuits. We named this plasticity "long-term plasticity of circuits" (LTPc) because it occurred in intact local circuits in vivo. To determine whether these changes were selective for a specific neuronal group versus affecting the global network, we monitored Ca^{2+} signals by activating neurons proximal to the selected group of neurons that were not subjected to glutamate photolysis. When the control neurons were activated, we did not observe a significant increase in Ca^{2+} amplitude in the selected group (Fig. 3*E* and *SI Appendix*, Table S2; $P > 0.1$). These findings indicate that increases in network responsiveness are not encoded in a random fashion but are somewhat specific for neurons highly active during the uncaging sequence. Because the chance of activating layer 5 neurons by glutamate uncaging is very low (Fig. 2 *C* and *D*), it is presumed that major connectivity changes were made through the layer 2/3 network, as supported by relatively high connection probability between layer 2/3 neurons in the somatosensory cortex (10).

These results also discard the possibility that the changes in fluorescence in the selected group of neurons were derived from nonspecific glutamate spillover. To confirm this, we performed glutamate uncaging with the same number of neurons at the same interval (10 ms) but 3 μm away from the cell body. With this setup, the amount of released glutamate should be the same as in the previous experiment, but APs should not be triggered (Fig. 1*E*). In this experiment, however, we did not detect a noticeable increase in Ca^{2+} response from the group of neurons (*SI Appendix*, Fig. S2). Within the selected group of neurons, the stimulation paradigm produced no noticeable differences in the magnitude of Ca^{2+} responses to direct uncaging, but there was a tendency for the network effects to diminish with sequence distance (Fig. 3*F*).

In parallel with changes in Ca^{2+} responses, we verified the expression of LTPc by electrophysiological recording (Fig. 4 *A*–*C*).

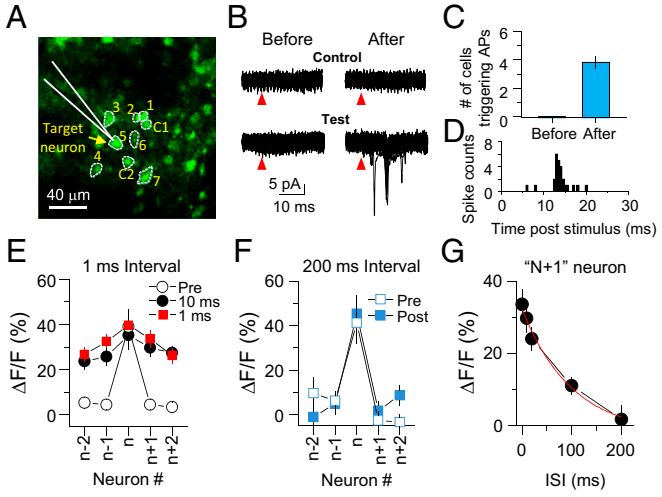

Fig. 4. Spike timing is critical for the induction of LTPc. (*A*) Representative image showing target cell recording and neighboring neurons that were activated by glutamate photolysis. The numbers were given randomly and APs were sequentially evoked from low to high number during multiple spike trains. C indicates a control neuron. Arrow indicates a target neuron recorded by a glass pipette (white). (*B*) Superimposed cell-juxtaposed electrophysiological recording traces from the target cell by activating neurons 1–7 or control neurons. Red arrowheads indicate glutamate uncaging. (*C*) Summary graph showing changes in the number of neurons triggering APs in the target neuron after multiple spike trains. (*D*) Peristimulus time histogram (PSTH) graph of AP spikes. (*E* and *F*) Δ*F*/*F* before and after spike trains at 1-ms (*E*) and 200-ms interstimulus intervals (ISIs) (*F*) are plotted. Summary plots of Ca^{2+} amplitude changes analyzed in the same way as shown in Fig. 2*D*. (*G*) Δ*F*/*F* of n+1 at various interspike-train intervals. Error bars indicate SEM.

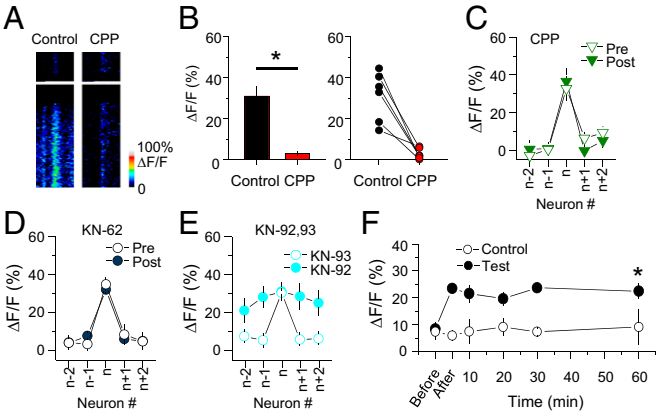

Fig. 5. Molecular mechanisms underlying LTPc induction. (*A*) Ca^{2+} transients were triggered in dendritic spines by glutamate photolysis in anesthetized mice and significantly blocked by CPP. (*B*) Summary and individual experimental plot of Δ*F*/*F* before and after CPP application. (*C*–*E*) Fluorescence changes after multiple spike trains in the presence of CPP, KN-62, KN-92, and KN-93. (*F*) Long-lasting modification of Ca^{2+} responses after the induction of LTPc. Individual target neurons were activated once every 10 min during the monitoring period and Δ*F*/*F* was measured from n+1 neurons. The averages of Δ*F*/*F* are plotted. Ca^{2+} responses were measured from the target neurons at 60 min (control, 60 min: 9.2 ± 6.7%, $n = 5$; test: 22.5 ± 3.0, $n = 17$, $P = 0.011$). n+1 neurons were designated as test neurons. * indicates statistical significance ($P < 0.05$) and error bars represent SEM.

We randomly chose seven neurons and performed juxtaposed cell recording from one neuron (target neuron) among this selected group of neurons. We then evoked APs in the other six neurons one by one and monitored whether triggering APs in these other neurons could drive firing in the initially chosen target neuron. Before multiple spike trains, no neuron was able to trigger firing in the target cell. However, after repetitive AP trains, triggering APs in the same population of neurons was able to induce APs in the target neuron (before: 0 neurons; after: 3.91 ± 0.31 out of six neurons; $n = 42$ neurons, $P < 0.001$) (Fig. 4*C*). The onset of APs was mostly detected between 10 and 20 ms after uncaging (Fig. 4*D*), suggesting that signals were relayed via polysynaptic connections. In addition, the AP onset time was not well-synchronized (about 10-ms jittering). This broad jittering window might indicate that the source of inputs did not originate from only one neuron. Together, these results strongly support that repetitive activation of a subgroup of neurons can induce circuit rearrangements that functionally link the stimulated neurons.

To test whether the induction of LTPc is dependent on spike timing between neurons, we stimulated neurons at various interstimulus intervals from 1 to 200 ms. Shorter intervals between spike trains reliably triggered changes in the fluorescence level in the group of neurons, but longer intervals (>100 ms) failed to trigger Ca^{2+} transients in neighboring neurons when APs were triggered in the target cell (Fig. 4 *E*–*G* and *SI Appendix*, Tables S3 and S4). These data imply that two different excitatory inputs arriving at layer 2/3 pyramidal neurons within a short time window give a higher chance for those neurons to be linked directly or indirectly and possibly make a functional subnetwork.

LTPc Is Dependent on NMDA Receptor and CaMKII Activation and Is Long-Lasting. The dependence on spike timing suggested that LTPc also requires time-locked coincident synaptic inputs via NMDA receptor activation in the target neuron. To test this hypothesis, we repeated the above experiments in the presence of the NMDA receptor antagonist CPP. APs were triggered normally by glutamate uncaging in the presence of CPP (Fig. 1*H*), but Ca^{2+} influx through NMDA receptors at individual synapses was completely blocked (Fig. 5 *A* and *B*). Blockade of synaptic Ca^{2+} influx

by inhibiting NMDA receptor activation also prevented the induction of LTPc (Fig. 5*C* and *SI Appendix*, Table S5; $P > 0.1$). A similar NMDA receptor-dependent circuit reorganization was recently reported in the visual cortex of anesthetized animals (28). Inhibiting a downstream signal of the NMDA receptor CaMKII by KN-62 or KN-93 (but not an inactive analog of KN-93) also prevented functional circuit reorganization (Fig. 5 *D* and *E* and *SI Appendix*, Table S6; $P > 0.1$). Thus, the glutamate photolysis-induced modification of functional connectivity in the network was dependent on plasticity triggered by NMDA receptor and CaMKII activation.

To determine whether LTPc is long-lasting, we monitored uncaging-evoked fluorescence-level changes for 1 h. We found that significantly elevated Ca^{2+} responses lasted for the full hour (Fig. 5*F*). These results indicate that the circuit reorganization triggered in this study is not just a periodic cortical state change such as up–down states but instead is a long-lasting modification of connectivity.

LTPc Is Dependent on the Number of Active Neurons. How does sequential neuronal firing lead to rearrangement of functional connectivity? What is the pattern of connectivity changes? One possibility is that the direct monosynaptic connections among neurons might be strengthened when repetitive APs are triggered in both neurons (*SI Appendix*, Fig. S3*A*). In this case, randomly chosen neurons would be initially synaptically connected but with connections too weak to trigger APs in other neurons. Repetitive spike trains induced by glutamate uncaging would then strengthen these synaptic connections enough to reach the AP threshold. A second possibility is that the axons and dendrites of the stimulated neurons are densely mingled and close enough to make new synaptic connections, such that multiple trains of APs create de novo functional synapses among stimulated neurons (29). A third possibility is that the effects are not limited to changes in the strength of synaptic connections among the stimulated neurons but reflect changes in a broader network of neurons in which the stimulated neurons participate (*SI Appendix*, Fig. S3*B*). In this scenario, there may be a preexisting pattern of connections that the stimulated neurons share that is strengthened by stimulation. Alternatively, stimulation could induce the formation of new connections in the network—of which the net effect is to augment the strength of the response in groups of neurons that fire together.

To examine these possibilities, we triggered spike trains in only a few neurons, allowing us to test direct monosynaptic changes without causing large network activation. If the fluorescence change is due to strengthened preexisting or newly made monosynaptic connections, the probability of detecting Ca^{2+}-level changes after repetitive spike trains should be similar when only two or three neurons are activated. However, when we triggered a short burst of firing on three neurons, we did not find coincidental firing on other neurons (Fig. 6*A* and *SI Appendix*, Table S7; $P > 0.1$). Thus, although these results do not discard the possibility of direct monosynaptic changes, the increase in probability of firing together shown in Fig. 3*D* is not fully explained by the potentiation of existing synaptic strength among neurons or from the formation of new connections directly linking neurons within the group.

It is possible that multiple trains of firing from a subset of neurons evoked broad activation of neuronal networks and led to a functional network rearrangement in the direction of connecting neurons indirectly. If broad network activity were involved through successive indirect polysynaptic activation, the capacity of incorporating network activity into the target neuron would increase when more neurons fire. For example, the percentage of inputs arriving at one target neuron would become higher when more neurons in the network are active. This assumption predicts that the possibility of functional circuit rearrangement becomes higher when more neurons are active. To test this idea, we varied the number of neurons. Consistent with

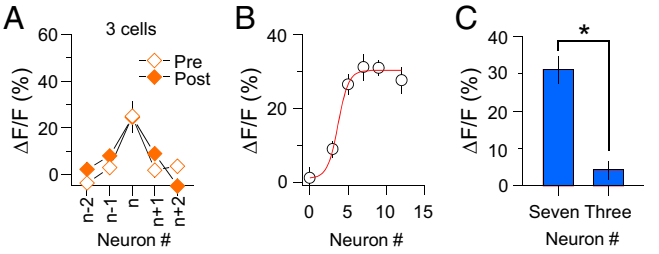

Fig. 6. LTPc is dependent on the number of active neurons. (*A*) $\Delta F/F$ was plotted when three neurons were activated. (*B*) Magnitude of Ca^{2+} response change depending on the number of activating neurons. The magnitude of $\Delta F/F$ was analyzed when repetitive spike trains were evoked in different numbers of neurons (0, 3, 5, 7, 9, and 12 neurons). Significant changes in Ca^{2+} responses were detected when a higher number of neurons was activated (0 neurons: 1.12 ± 2.9%; 3 neurons: 8.9 ± 2.2%; 5 neurons: 26.4 ± 2.7%; 7 neurons: 31.1 ± 3.7%; 9 neurons: 30.9 ± 2.2%; 12 neurons: 27.6 ± 3.6%). (*C*) The same number of glutamate photolyses was given when seven or three neurons were chosen. Summary graph of fluorescence changes after multiple spike trains (seven neurons: 31.1 ± 3.7%, $n = 19$; three neurons: 4.29 ± 2.4%, $n = 15$; $P < 0.001$). * indicates statistical significance ($P < 0.05$) and error bars represent SEM.

our hypothesis, the fluorescence-level change in the selected neurons was significantly increased as the number of neurons increased (Fig. 6*B*). Because each neuron received the same number of photolysis reactions, the total number of uncaging events was less when a low number of neurons was chosen. To determine whether the lack of fluorescence changes in three neurons was due to the reduced number of uncaging events, we increased the number of uncaging events for each neuron to match the total number of uncaging events as for seven activated neurons. With this setup, we still did not observe similar fluorescence changes when three neurons were chosen (seven neurons, $\Delta F/F$: 31.1 ± 3.73%, $n = 19$; three neurons, $\Delta F/F$: 4.3 ± 2.42%, $n = 15$; $P < 0.005$) (Fig. 6*C*). These data suggest that coincident firing from a certain number of neurons is crucial for building functional microcircuits.

LTPc Caused Changes in Both the Number and Firing Rate of Neurons in the Network. It has been reported that the probability of local connections among excitatory pyramidal neurons is distance-dependent (5, 30–32); that is, the closer that neurons are located to each other, the higher the probability of connectivity. We examined whether the direction of neuronal connectivity is determined by the temporal order of activity or by the physical distance between two neurons. First, to determine whether LTPc depends on the distance between neurons, we reanalyzed the Ca^{2+} levels in different neuronal groups as a function of distance from the target neurons. Because most of the neurons we picked were located close to each other (Fig. 3*A*), the majority of neurons were localized within 30 μm from the target neuron. Several neurons were chosen farther than 100 μm from the target neuron, but we could not find any differences in Ca^{2+}-level change within the imaging boundary of 150 μm, suggesting that the formation of neuronal group firing together does not have a distance limit, at least up to 150 μm (Fig. 7*A*). In another set of experiments, we randomized the order of activation, so that the distance between target neurons and "n+1" or "n−1" neurons was not close to each other (the target neuron was always called "n") (Fig. 7*B*). This randomized sequential activation still showed a similar symmetric profile of fluorescence changes, as shown in Fig. 3*D*. These results strengthen the conclusion that distance among neurons within a 150-μm window is not critical during circuit reorganization (Fig. 7*C*).

To visualize whether reorganization of functional connectivity was made in a random fashion, we performed a whole-frame

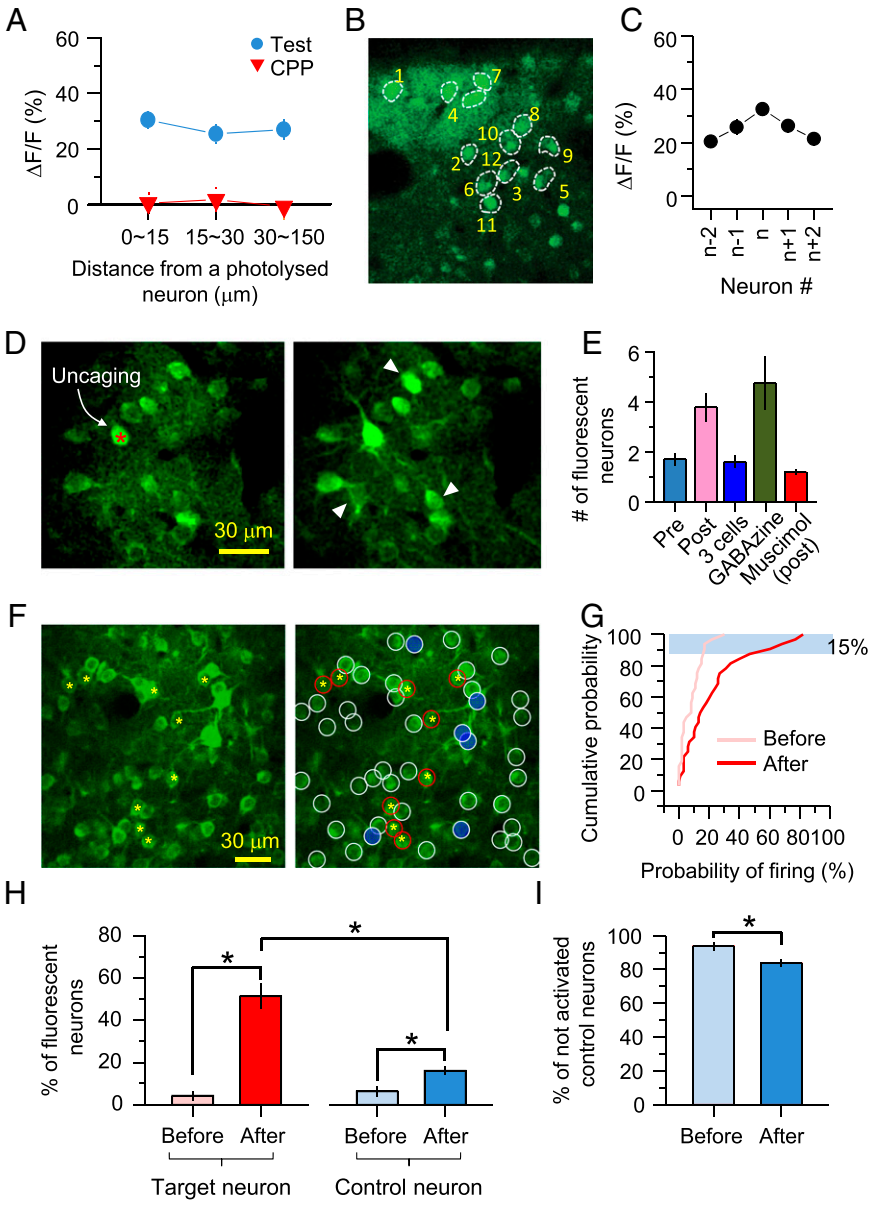

Fig. 7. Network plasticity subserves functional circuit reorganization. (*A*) Δ*F*/*F* shown in Figs. 2*D* and 4*C* was reanalyzed by distance. Neurons were divided into three groups by distance (<15 μm, 15~30 μm, and >30 μm). (*B*) Representative image of randomized sequential activation of a group of neurons as shown by number. (*C*) Δ*F*/*F* after multiple spike trains in a random order. (*D*) A frame scan revealed that triggering APs on single neurons induced firing on neighboring neurons after multiple spike trains. (*Right*) An image taken 1 s after glutamate uncaging. Arrowheads indicate newly fluorescent neurons. (*E*) Average number of neurons showing fluorescence changes by single-cell activation (pre: 1.7 ± 0.26, $n = 20$; post: 3.8 ± 0.57, $n = 20$; $P < 0.05$ compared with pre; three cells: 1.6 ± 0.25, $n = 15$, $P > 0.5$ compared with pre; GABAzine: 4.8 ± 1.06, $n = 15$, $P < 0.1$ compared with pre; muscimol: 1.2 ± 0.11, $n = 15$, $P < 0.05$ compared with post). (*F*) Sample image of a neuronal population for LTPc induction. Red circled neurons represent the selected target neurons that were subjected to repetitive sequential glutamate uncaging. Neurons with white circles are near control neurons, and the top 15% of control neurons showing the highest successful Ca^{2+} transients are colored blue. (*G*) Cumulative plot of firing probability before and after LTPc induction. Blue-colored neurons shown in *F* are masked by a blue rectangle ($n = 32$ control neurons). (*H*) Average graph of percentile changes of fluorescent neurons before and after LTPc (6 mice, 6 groups, 7–12 target neurons, and 30–40 control neurons in each group). (*I*) Percentage of quiet (not activated) control neurons before and after LTPc. *$P < 0.05$; error bars represent SEM.

scan to detect any changes of Ca^{2+} transients in all neurons within an imaging window (150 × 150 μm) (Fig. 7*D*). We observed a significant increase in the number of neurons that became newly fluorescent after LTPc induction (Fig. 7*E*). These data are consistent with the third hypothesis that the pattern of functional connections in a network is specifically rearranged or formed in a direction toward increasing the strength of response in groups of neurons that are activated together (*SI Appendix*, Fig. S3*B*). Further supporting that broad network activity arises during LTPc, we found that boosting network activation by blocking $GABA_A$ receptors with GABAzine showed a similar increase of newly fluorescent neurons even without triggering multiple spike trains. Conversely, preventing network activation by muscimol inhibited the increase of newly fluorescent neurons after AP trains (Fig. 7*E*).

To systematically analyze network connectivity changes, we performed a set of experiments monitoring a large number of control neurons (Fig. 7*F*). We selected 9–12 target neurons to

induce LTPc and monitored Ca^{2+} transients from more than 30 control neurons in the network. After LTPc induction, when an individual target neuron was activated, the probability of firing in control neurons was significantly increased, indicating again that nearby unstimulated neurons are newly recruited into the circuit of the activated group. Interestingly, the pattern of connections did not appear to be equal among neurons. Some neurons were activated more often than others, with 10% of control neurons in the network showing roughly a 50% probability of firing and the remaining 90% firing at less than 40%. In particular, about 40% of total control neurons showed less than a 10% success rate. This finding implies that LTPc can increase not only the number of active neurons in the network but also the firing frequency of individual neurons. In addition, the number of newly fluorescent neurons was significantly increased after LTPc induction in both target neurons and neighboring control neurons (Fig. 7*H*) (target neurons, before: 4.4 ± 2.3%, after: 51.4 ± 6.1%; control neurons, before: 6.2 ± 2.5%, after: 16.2 ± 2.1%; six mice, six groups, $P < 0.01$). Related to these findings, the number of "not" activated control neurons was significantly reduced (Fig. 7*I*) (before: 93.8 ± 2.5%, after: 83.8 ± 2.1%; six mice, six groups, $P < 0.05$). The majority of control neurons were not active, but about 10% of control neurons appeared to be newly recruited to the activated target group of neurons.

The newly fluorescent neurons did not show any noticeable direction selectivity from the target neurons, suggesting that a new network can be established toward multiple directions (Fig. 8*A*). We also examined the effect on LTPc of enhancing or suppressing network activation by GABAzine or muscimol, respectively. Blocking inhibition (with GABAzine) did not affect the induction of LTPc; however, inhibiting network activation (with muscimol) completely blocked LTPc (Fig. 8*B* and *SI Appendix*, Tables S8 and S9; GABAzine: $P < 0.05$; muscimol: $P > 0.1$).

Although we did not find physical directionality of newly fluorescent neurons, functional connectivity may still be reorganized toward a direction to build a functional subnetwork. Because the level of network activity is gradually increased during sequential activation of neurons, the probability of coincident AP firing would be higher in neurons activated later in sequence (Fig. 8*C*). This scenario predicts that synaptic strength changes evoked from spike trains in circuits are made in the same direction as the activation sequence. Indeed, when we photolyzed glutamate in five newly fluorescent neurons, the success rate of evoking Ca^{2+} transients in an originally selected group of neurons became higher toward the end of the sequence (Fig. 8*D*). Thus, neuronal connectivity in a microcircuit is likely to be built in a directional manner. These results suggest that time-sensitive sensory information from the periphery formulates neural circuit assembly asymmetry.

Discussion

In this study, we examined how the degree and directionality of functional connectivity among layer 2/3 neurons in the mammalian cortex are influenced by neuronal activity, and how the results integrate into sensory information processing. During cortical circuit development in the mammalian brain, functional microcircuits form from groups of excitatory neurons receiving similar sensory information (33–37). The emergence of functional populations is not limited to the sensory cortex but also occurs in other subcortical areas during normal development or learning, a phenomenon that is increasingly acknowledged as a general characteristic of neural coding in the mammalian brain (38–43). Presumably, changes in synaptic strength and/or modification of neuronal connectivity underlie this process, but we lack a systematic understanding of circuit rearrangement at a multineuron level. We addressed this fundamental question using electrophysiological and optical approaches that allowed

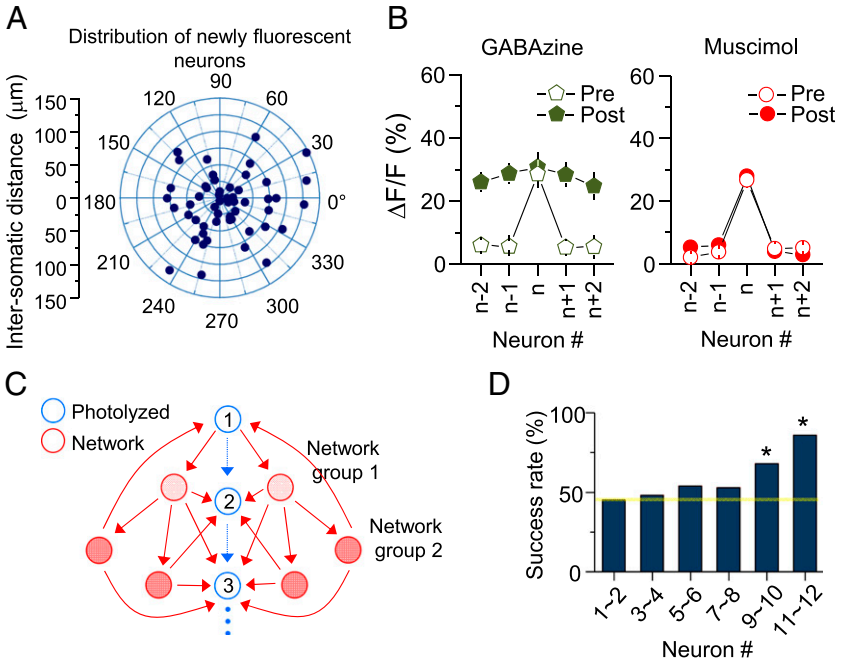

Fig. 8. Directional connectivity induced by sequential activation of neurons. (*A*) Distribution and distance of newly fluorescent neurons. (*B*) Summary plots of $\Delta F/F$ in the presence of GABAzine (200 μM) and muscimol (10 mM). (*C*) Schematic drawing of potential network activity spread during sequential neuronal activation. Arrows indicate possible neuronal connections, and blue neurons were a group of neurons that received sequential glutamate uncaging. (*D*) Success rate comparison among neurons in the selected group. Glutamate uncaging was given to five neighboring neurons in the network, and successful Ca^{2+} transients were monitored from an originally selected group of neurons (23 mice; 1~2 neurons: 46%; 9~10 neurons: 69%; $P < 0.05$ compared with 1~2 neurons; 11~12 neurons: 78% success rate; $P < 0.05$ compared with 1~2 neurons). *$P < 0.05$; error bars represent SEM.

us to manipulate and monitor neuronal activity at single-cell resolution. Using these methods, we studied the cellular underpinnings of functional microcircuit reorganization in layer 2/3 of the somatosensory cortex.

Imaging Network Plasticity at Single-Cell Resolution. Our data showed that repetitive triggering of spike trains in layer 2/3 pyramidal neurons in the somatosensory cortex led to the formation of a neuronal group that fired together through network activation. To visualize the pattern of neuronal connectivity changes at single-cell resolution in the cortical network, we addressed two important issues. First, we attempted to study intact brain circuits. Cortical pyramidal neurons are densely interconnected and often project their axons to other cortical columns or even other brain areas. These dense local connections and long projections are severely disrupted in brain slices, and thus render studies of the scope or directionality of circuit plasticity incomplete. More importantly, functional in vivo circuit mechanisms underlying sensory perception or manipulation are difficult to investigate from slice experiments. To avoid this limitation, we implemented cutting-edge techniques that enabled us to simultaneously control and monitor neuronal activity in intact cortical circuits. We developed a microfluidic in vivo chamber through which caged compounds and other pharmacological drugs could circulate. The top of the chamber was covered with a glass coverslip to prevent evaporation of brain fluid and enabled imaging and uncaging through the glass window. The thinness of the chamber (500 μm) permitted high-resolution imaging with minimal degradation of signal (*SI Appendix*, Fig. S4, *Right*). Using this highly sensitive approach, we could study network plasticity without impairing brain circuits.

The second key issue was using techniques that allowed us to manipulate activity at the single-cell level. Simultaneous control of large populations of neurons does not allow us to identify the timing-dependent mechanisms of neuronal connectivity changes. Temporally unequal inputs into the cortex may influence neuronal connectivity, thereby rendering cortical circuit assembly asymmetric. Previous work suggested that the sensitivity to the temporal input sequence was related to feature detection and the mode of neural coding of speed and directionality propagating in the cortex (44, 45). Two-photon photostimulation of glutamate made it possible to control neuronal activity with millisecond accuracy. With the high temporal resolution offered by this technique, we demonstrated that timing between spikes is important for plasticity in network connectivity.

Spike Timing Dependency in Neural Circuits. The STDP rule predicts that synaptic strength in a neuron that receives excitatory inputs 10 ms after the target neuron (n+1) will be potentiated. Indeed, we found that the magnitude of Ca^{2+} responses was significantly increased (Fig. 3*D*). However, we also detected a noticeable increase in Ca^{2+} response in neurons for which APs were triggered 10 ms before the target neuron (n−1). According to the STDP rule, if n−1 neurons receive synaptic inputs directly from a target neuron, long-term depression is to be expected between these two neurons. Then, how was the long-term increase of Ca^{2+} in n−1 neurons elicited? One possibility is that the plasticity-inducing paradigm used in this study evoked recurrent cortical network activity that was propagated back to a group of neurons that were photolyzed. In this scenario, n−1 neurons may have received indirect excitatory inputs within a window of tens of milliseconds, so the pattern of spiking in n−1 neurons may have become similar to the pattern occurring in n+1 or n+2 neurons. In particular, neuronal spike patterns in vivo are more complex than in vitro, so the directionality of activity-dependent synaptic modification does not strictly follow an STDP rule such as potentiation in pre→post cell activation or depression in post→pre activation (46). Thus, STDP at the circuit level is more complicated than between two neurons.

Another possibility is the partial blockade of inhibition by caged glutamate. MNI (4-Methoxy-7-nitroindolinyl)-Glu is known to block $GABA_A$ receptors (47). To minimize this potential problem, we used CDNI-Glu, which is approximately five times more potent than MNI-Glu. We could therefore use a much lower concentration that has minimal inhibitory action on $GABA_A$ receptors and does not cause firing pattern change (18, 48). In our experimental conditions, it was difficult to predict the exact final concentration of caged glutamate in vivo, but potential disinhibition by CDNI-Glu may have changed the magnitude of Ca^{2+} rise in local dendritic spines and facilitated LTP in the network (49–51).

Physiological Relevance. In most previous studies, sparse spiking and distributed sensory-evoked responses over a long interval were mainly observed by electrophysiological recordings or Ca^{2+} imaging evoked by stimulation with a single whisker or a few whiskers. However, freely behaving mice use many whiskers at high frequency (10–20 Hz) to explore external objects (52–54). Furthermore, each external object is contacted by multiple whiskers in a short interval (generally much faster than 20 Hz) in sequence. Neuronal activity analysis during active whisking in freely moving animals has not yet been well-demonstrated. Recently, other investigators have shown that a population of neurons activated by different whiskers is localized in one barrel area (equivalent to or smaller than the size of our imaging window) (7, 55–57). If this were the case, a series of multiple-whisker stimulations at short interstimulus intervals would cause spiking at different layer 2/3 neurons in sequence at short intervals, a situation that may be similar to our experimental protocol and is likely to occur in freely moving animals.

Furthermore, a recent study using multiple-whisker deflection demonstrated that spiking latency is slightly different (about 10 ms) depending on the direction of whisking (caudal vs. rostral) (58). These results also demonstrated that such a short time separation of spikes carries meaningful sensory information. Last, physiological relevance of LTPc in this study does not have to be limited in the context of sensory stimuli. Other inputs, such as top–down signals from the motor cortex, come into layer 2/3 neurons. These inputs, at least in part, should contribute to the reorganization of circuits. Thus, our study will be helpful in understanding cellular mechanisms by which neurons in the sensory cortex integrate various sources of cortical inputs.

Experimental Procedures

Animals and Surgical Procedures. All experiments were performed in accordance with protocols approved by the Institutional Animal Care and Use Committee of the Max Planck Florida Institute for Neuroscience and National Institutes of Health guidelines. C57BL/6 mice (Charles River Laboratories) were anesthetized with a mixture of ketamine (80 mg/kg) and xylazine (15 mg/kg) (Sigma-Aldrich). Adeno-associated virus (300 nL) containing the GCaMP6f gene, which follows the synapsin promoter (AV-1-PV2822; University of Pennsylvania Gene Therapy Program Vector Core), was injected into layer 2/3 primary somatosensory cortex at postnatal days 11–13. Two to three weeks after viral injection, these C57BL/6 mice were anesthetized with 5% (vol/vol) isoflurane for induction and the same anesthetic mixture dosage as used in virus injection for maintenance. An ∼2- to 3-mm craniotomy was made at the virus-injected area, and the custom-designed in vivo microchamber was implanted onto the skull right around the craniotomy site and fixed by dental cement. This microchamber was made out of titanium and was not reused after the experiment. First, a series of circular holes with the inside of diameter was cut in titanium metal sheet. We cut them into small square chips using sheet-metal shears, and then cut the edge of the square to make a circular ring shape with the inside diameter, 2.1 mm, and the outside diameter, 2.7 mm. The microchamber was connected with thin tubes (wall, 75 μm; inner diameter, 150 μm; Zeus) and CDNI-glutamate and pharmacological drugs were perfused through these tubes at a speed of 50∼100 μL/min. For electrophysiological recording, a larger microchamber was used (inner diameter, 3 mm) and a cover glass did not cover the chamber for electrode access. A titanium head-holder adaptor was affixed

onto the microchamber with glue [Loctite 454 (Henkel)], and the mouse head was stably fixed to the head post. Mouse body temperature was consistently kept at 36–37 °C with a homeothermic blanket system with a flexible probe (Harvard Apparatus) during animal surgery and imaging experiments.

Slice Culture. Organotypic cortical slice cultures were prepared from 3-d-old C57BL/6 mice. The brain was removed and immediately immersed in chilled and oxygenated dissection media. The cortex was sliced at 400-μm thickness and, on a sterile culture plate insert, three slices were placed per well in six-well plates with prewarmed slice culture media. Experiments were performed at days in vitro 22–26.

Two-Photon Microscope Ca^{2+} Imaging and Uncaging. We used a combined two-photon laser-scanning microscopy and two-photon laser photoactivation system purchased from Prairie Technologies. Two mode-locked Ti:sapphire lasers (MaiTai HP and MaiTai HP DeepSee; Newport Spectra-Physics) were used for uncaging and imaging at wavelengths of 720 and 910 nm, respectively. Laser power for imaging was set at 5∼10 mW, and uncaging laser power was normally used at a range of 15∼25 mW to trigger action potentials at individual neurons. The typical depth of target neurons was 100∼200 μm from the surface of the brain. Total photolysis volume was increased by making a beam size underfilled to the back aperture of the objective lens [16×, 0.8 NA, WD (working distance) 3 mm] by 40% as similarly shown in a previous report (21). In most cases, neurons did not move at all under the anesthetized state, but in a case in which Ca^{2+} signals were moving by pulsation more than 1 μm (*SI Appendix*, Fig. S4), we did not perform imaging and uncaging. Percent change of $\Delta F/F$ was calculated by averaging all responses, including failures. When CPP, KN-62, and KN-93 were applied to block NMDA receptors and CaMKII, glutamate uncaging was initiated at least 15 min after application. Photomultiplier tubes (7422P-40 GaAsP; Hamamatsu) were used for fluorescence image detection. Fluorescent cells in a bright field were identified by epifluorescence (X-cite 120; Lumen Dynamics) scanned by a digital CCD camera (QIClick-F-M-12; QImaging). Data acquisition was done with Prairie View and TriggerSync software (Prairie Technologies).

For glutamate uncaging, 2.5 mM CDNI-glutamate (synthesized by Shanghai Medicilon) in artificial cerebrospinal fluid (ACSF) was perfused and circulated by peristaltic pump. Fifteen units of glutamic-pyruvic transaminase (Sigma-Aldrich) and 2 mM sodium pyruvate (Sigma-Aldrich) was also added to increase glutamate uptake. Line scan crossing the center of cell bodies was performed to measure Ca^{2+} fluorescence changes. Ca^{2+} images were analyzed as $\Delta F/F$ in ImageJ (NIH) and plotted with Origin software (OriginLab Corp.).

LTPc induction protocols were as follows. Before the induction of LTPc, a group of neurons (usually 7–12) was randomly selected and each neuron was activated with a 2-ms-duration laser at 720 nm one by one to monitor baseline Ca^{2+} transients from the selected group. To trigger LTPc, sequential activation (from neuron 1–7 in the case of seven neurons) was repeated consecutively three times in the same order followed by a 2-min rest. These 3 sequential activations/2-min rest intervals (one cycle) were repeated 15 times for a total of 45 (3×15) sequential activations. Ten minutes after the induction protocol, Ca^{2+} transients were monitored again from the same group of neurons by activating individual neurons one by one. For long-term monitoring of correlated activity, fluorescence level was monitored every 10 min up to 60 min by activating each neuron.

Electrophysiology. CDNI-glutamate and all pharmacological drugs were dissolved in ACSF containing 127 mM NaCl, 25 mM $NaHCO_3$, 1.25 mM NaH_2PO_4, 2.5 mM KCl, 25 mM glucose, 1 mM $MgCl_2$, and 2 mM $CaCl_2$. Glass pipettes (8–12 MΩ) were pulled by micropipette puller (P-1000; Sutter Instrument) and filled with internal solution: 135 mM $KMeSO_4$, 5 mM KCl, 5 mM Hepes, 4 mM MgATP, 0.3 mM Na_2GTP, and 10 mM phosphocreatine (pH 7.3). All recordings were made with MultiClamp700B (Axon Instruments) and data were analyzed and plotted with Clampfit 10.3 (Molecular Devices) and Origin.

Pharmacology and Statistics. CPP, NBQX, KN-62, GABAzine, muscimol, and TTX were purchased from Tocris. KN-92 and KN-93 were obtained from EMD Millipore. Data are presented as ±SEM unless otherwise stated. Paired or unpaired two-tailed Student's *t* tests were used to determine statistical significance as indicated by asterisks. Fisher's exact test was used to determine the level of significance of the success rate of Ca^{2+} transients shown in Fig. 8*D*. $P < 0.05$ was judged as significant.

ACKNOWLEDGMENTS. We thank all members of the H.B.-K. laboratory. We also thank D. Fitzpatrick, B. L. Sabatini, R. Yasuda, H. Taniguchi, N. X. Tritsch, and B. Sakmann for their constructive comments on the initial manuscripts. We thank J. Schummers and L. Yan for help in setting up in vivo animal surgeries and with the two-photon microscope setup. GCaMP6f virus was available from the Genetically-Encoded Neuronal Indicator and Effector (GENIE) Project and the Janelia Farm Research Campus, especially V. Jayaraman, R. A. Kerr, D. S. Kim, L. L. Looger, and K. Svoboda. This work was supported by funding from the Max Planck Florida Institute for Neuroscience (to H.-B.K.) and R01 MH107460 (to H.-B.K.).

1. Ahissar E, Sosnik R, Haidarliu S (2000) Transformation from temporal to rate coding in a somatosensory thalamocortical pathway. *Nature* 406(6793):302–306.
2. Armstrong-James M, Fox K (1987) Spatiotemporal convergence and divergence in the rat S1 "barrel" cortex. *J Comp Neurol* 263(2):265–281.
3. Armstrong-James M, Fox K, Das-Gupta A (1992) Flow of excitation within rat barrel cortex on striking a single vibrissa. *J Neurophysiol* 68(4):1345–1358.
4. Simons DJ (1978) Response properties of vibrissa units in rat SI somatosensory neocortex. *J Neurophysiol* 41(3):798–820.
5. Feldmeyer D, Lübke J, Sakmann B (2006) Efficacy and connectivity of intracolumnar pairs of layer 2/3 pyramidal cells in the barrel cortex of juvenile rats. *J Physiol* 575(Pt 2):583–602.
6. Wilbrecht L, Holtmaat A, Wright N, Fox K, Svoboda K (2010) Structural plasticity underlies experience-dependent functional plasticity of cortical circuits. *J Neurosci* 30(14):4927–4932.
7. Sato TR, Gray NW, Mainen ZF, Svoboda K (2007) The functional microarchitecture of the mouse barrel cortex. *PLoS Biol* 5(7):e189.
8. Jouhanneau JS, et al. (2014) Cortical fosGFP expression reveals broad receptive field excitatory neurons targeted by POm. *Neuron* 84(5):1065–1078.
9. Varga Z, Jia H, Sakmann B, Konnerth A (2011) Dendritic coding of multiple sensory inputs in single cortical neurons in vivo. *Proc Natl Acad Sci USA* 108(37):15420–15425.
10. Lefort S, Tomm C, Floyd Sarria JC, Petersen CC (2009) The excitatory neuronal network of the C2 barrel column in mouse primary somatosensory cortex. *Neuron* 61(2): 301–316.
11. Brecht M, Roth A, Sakmann B (2003) Dynamic receptive fields of reconstructed pyramidal cells in layers 3 and 2 of rat somatosensory barrel cortex. *J Physiol* 553(Pt 1): 243–265.
12. Brecht M, Sakmann B (2002) Dynamic representation of whisker deflection by synaptic potentials in spiny stellate and pyramidal cells in the barrels and septa of layer 4 rat somatosensory cortex. *J Physiol* 543(Pt 1):49–70.
13. Banerjee A, González-Rueda A, Sampaio-Baptista C, Paulsen O, Rodríguez-Moreno A (2014) Distinct mechanisms of spike timing-dependent LTD at vertical and horizontal inputs onto L2/3 pyramidal neurons in mouse barrel cortex. *Physiol Rep* 2(3):e00271.
14. Feldman DE (2012) The spike-timing dependence of plasticity. *Neuron* 75(4):556–571.
15. Sjöström PJ, Turrigiano GG, Nelson SB (2001) Rate, timing, and cooperativity jointly determine cortical synaptic plasticity. *Neuron* 32(6):1149–1164.
16. Song S, Abbott LF (2001) Cortical development and remapping through spike timing-dependent plasticity. *Neuron* 32(2):339–350.
17. Chen TW, et al. (2013) Ultrasensitive fluorescent proteins for imaging neuronal activity. *Nature* 499(7458):295–300.
18. Ellis-Davies GC, Matsuzaki M, Paukert M, Kasai H, Bergles DE (2007) 4-Carboxymethoxy-5,7-dinitroindolinyl-Glu: An improved caged glutamate for expeditious ultraviolet and two-photon photolysis in brain slices. *J Neurosci* 27(25):6601–6604.
19. Ashby MC, Isaac JT (2011) Maturation of a recurrent excitatory neocortical circuit by experience-dependent unsilencing of newly formed dendritic spines. *Neuron* 70(3): 510–521.
20. Fino E, Yuste R (2011) Dense inhibitory connectivity in neocortex. *Neuron* 69(6): 1188–1203.
21. Matsuzaki M, Ellis-Davies GC, Kasai H (2008) Three-dimensional mapping of unitary synaptic connections by two-photon macro photolysis of caged glutamate. *J Neurophysiol* 99(3):1535–1544.
22. Akerboom J, et al. (2012) Optimization of a GCaMP calcium indicator for neural activity imaging. *J Neurosci* 32(40):13819–13840.
23. Tian L, et al. (2009) Imaging neural activity in worms, flies and mice with improved GCaMP calcium indicators. *Nat Methods* 6(12):875–881.
24. Sjöström PJ, Rancz EA, Roth A, Häusser M (2008) Dendritic excitability and synaptic plasticity. *Physiol Rev* 88(2):769–840.
25. Tsodyks MV, Markram H (1997) The neural code between neocortical pyramidal neurons depends on neurotransmitter release probability. *Proc Natl Acad Sci USA* 94(2):719–723.
26. Meliza CD, Dan Y (2006) Receptive-field modification in rat visual cortex induced by paired visual stimulation and single-cell spiking. *Neuron* 49(2):183–189.
27. Bi GQ, Poo MM (1998) Synaptic modifications in cultured hippocampal neurons: Dependence on spike timing, synaptic strength, and postsynaptic cell type. *J Neurosci* 18(24):10464–10472.
28. Xu S, Jiang W, Poo MM, Dan Y (2012) Activity recall in a visual cortical ensemble. *Nat Neurosci* 15(3):449–455.
29. Kwon HB, Sabatini BL (2011) Glutamate induces de novo growth of functional spines in developing cortex. *Nature* 474(7349):100–104.
30. Holmgren C, Harkany T, Svennenfors B, Zilberter Y (2003) Pyramidal cell communication within local networks in layer 2/3 of rat neocortex. *J Physiol* 551(Pt 1):139–153.

31. Perin R, Berger TK, Markram H (2011) A synaptic organizing principle for cortical neuronal groups. *Proc Natl Acad Sci USA* 108(13):5419–5424.
32. Song S, Sjöström PJ, Reigl M, Nelson S, Chklovskii DB (2005) Highly nonrandom features of synaptic connectivity in local cortical circuits. *PLoS Biol* 3(3):e68.
33. Albright TD, Desimone R, Gross CG (1984) Columnar organization of directionally selective cells in visual area MT of the macaque. *J Neurophysiol* 51(1):16–31.
34. Fujita I, Tanaka K, Ito M, Cheng K (1992) Columns for visual features of objects in monkey inferotemporal cortex. *Nature* 360(6402):343–346.
35. Hafting T, Fyhn M, Molden S, Moser MB, Moser EI (2005) Microstructure of a spatial map in the entorhinal cortex. *Nature* 436(7052):801–806.
36. Hubel DH, Wiesel TN (1962) Receptive fields, binocular interaction and functional architecture in the cat's visual cortex. *J Physiol* 160:106–154.
37. Mountcastle VB (1957) Modality and topographic properties of single neurons of cat's somatic sensory cortex. *J Neurophysiol* 20(4):408–434.
38. Bastos AM, et al. (2012) Canonical microcircuits for predictive coding. *Neuron* 76(4): 695–711.
39. Coulter DA, et al. (2011) Hippocampal microcircuit dynamics probed using optical imaging approaches. *J Physiol* 589(Pt 8):1893–1903.
40. Margolis DJ, Lütcke H, Helmchen F (2014) Microcircuit dynamics of map plasticity in barrel cortex. *Curr Opin Neurobiol* 24(1):76–81.
41. Shepherd GM, Katz DM (2011) Synaptic microcircuit dysfunction in genetic models of neurodevelopmental disorders: Focus on Mecp2 and Met. *Curr Opin Neurobiol* 21(6):827–833.
42. Turrigiano G (2011) Too many cooks? Intrinsic and synaptic homeostatic mechanisms in cortical circuit refinement. *Annu Rev Neurosci* 34:89–103.
43. van Welie I, Smith IT, Watt AJ (2011) The metamorphosis of the developing cerebellar microcircuit. *Curr Opin Neurobiol* 21(2):245–253.
44. Meister M, Lagnado L, Baylor DA (1995) Concerted signaling by retinal ganglion cells. *Science* 270(5239):1207–1210.
45. Wehr M, Laurent G (1996) Odour encoding by temporal sequences of firing in oscillating neural assemblies. *Nature* 384(6605):162–166.
46. Froemke RC, Dan Y (2002) Spike-timing-dependent synaptic modification induced by natural spike trains. *Nature* 416(6879):433–438.
47. Matsuzaki M, Hayama T, Kasai H, Ellis-Davies GC (2010) Two-photon uncaging of gamma-aminobutyric acid in intact brain tissue. *Nat Chem Biol* 6(4):255–257.
48. Alviña K, Walter JT, Kohn A, Ellis-Davies G, Khodakhah K (2008) Questioning the role of rebound firing in the cerebellum. *Nat Neurosci* 11(11):1256–1258.
49. Chiu CQ, et al. (2013) Compartmentalization of GABAergic inhibition by dendritic spines. *Science* 340(6133):759–762.
50. Gambino F, Holtmaat A (2012) Spike-timing-dependent potentiation of sensory surround in the somatosensory cortex is facilitated by deprivation-mediated disinhibition. *Neuron* 75(3):490–502.
51. Hayama T, et al. (2013) GABA promotes the competitive selection of dendritic spines by controlling local Ca^{2+} signaling. *Nat Neurosci* 16(10):1409–1416.
52. Mitchinson B, et al. (2011) Active vibrissal sensing in rodents and marsupials. *Philos Trans R Soc Lond B Biol Sci* 366(1581):3037–3048.
53. Sofroniew NJ, Cohen JD, Lee AK, Svoboda K (2014) Natural whisker-guided behavior by head-fixed mice in tactile virtual reality. *J Neurosci* 34(29):9537–9550.
54. Voigts J, Sakmann B, Celikel T (2008) Unsupervised whisker tracking in unrestrained behaving animals. *J Neurophysiol* 100(1):504–515.
55. Clancy KB, Schnepel P, Rao AT, Feldman DE (2015) Structure of a single whisker representation in layer 2 of mouse somatosensory cortex. *J Neurosci* 35(9): 3946–3958.
56. Kerr JN, et al. (2007) Spatial organization of neuronal population responses in layer 2/3 of rat barrel cortex. *J Neurosci* 27(48):13316–13328.
57. Margolis DJ, et al. (2012) Reorganization of cortical population activity imaged throughout long-term sensory deprivation. *Nat Neurosci* 15(11):1539–1546.
58. Le Cam J, Estebanez L, Jacob V, Shulz DE (2011) Spatial structure of multiwhisker receptive fields in the barrel cortex is stimulus dependent. *J Neurophysiol* 106(2): 986–998.